



OPEN ACCESS

EDITED BY

Chunyan Li,
Louisiana State University,
United States

REVIEWED BY

Eugene Morozov,
P.P. Shirshov Institute of Oceanology
(RAS), Russia
Xianqing Lv,
Ocean University of China, China

*CORRESPONDENCE

Ibrahim Hoteit
ibrahim.hoteit@kaust.edu.sa

SPECIALTY SECTION

This article was submitted to
Physical Oceanography,
a section of the journal
Frontiers in Marine Science

RECEIVED 08 June 2022

ACCEPTED 25 July 2022

PUBLISHED 17 August 2022

CITATION

Guo D, Yao F, Zhan P, Krokos G and
Hoteit I (2022) Hindrance effect of
tides on water exchanges between the
Red Sea and the Gulf of Aden.
Front. Mar. Sci. 9:964097.
doi: 10.3389/fmars.2022.964097

COPYRIGHT

© 2022 Guo, Yao, Zhan, Krokos and
Hoteit. This is an open-access article
distributed under the terms of the
[Creative Commons Attribution License
\(CC BY\)](https://creativecommons.org/licenses/by/4.0/). The use, distribution or
reproduction in other forums is
permitted, provided the original
author(s) and the copyright owner(s)
are credited and that the original
publication in this journal is cited, in
accordance with accepted academic
practice. No use, distribution or
reproduction is permitted which does
not comply with these terms.

Hindrance effect of tides on water exchanges between the Red Sea and the Gulf of Aden

Daquan Guo¹, Fengchao Yao^{1,2}, Peng Zhan^{1,3},
George Krokos¹ and Ibrahim Hoteit^{1*}

¹Department of Ocean Science and Engineering, King Abdullah University of Science and Technology, Thuwal, Saudi Arabia, ²School of Marine Sciences, Sun Yat-Sen University, Guangzhou, China, ³Department of Ocean Science and Engineering, Southern University of Science and Technology, Shenzhen, China

As a semienclosed marginal sea, the Red Sea connects with the open ocean through a narrow strait at its southern end, known as the Bab-al-Mandeb (BAM) strait. The water exchange between the Red Sea and the Gulf of Aden at the BAM strait is crucial for the water mass transformations and thermohaline circulation in the Red Sea as well as for nutrient supply to the open ocean. In this study, a three-dimensional high-resolution nonhydrostatic MIT general circulation model (MITgcm) was used to investigate the tidal influence on the water exchange in the BAM strait through simulations with and without tidal forcing. We found that the tidal effects on the water exchange in winter were insignificant; however, the summer intrusion of the Gulf of Aden Intermediate Water (GAIW) was strongly affected. When the simulation includes tidal forcing, the along-axis northern extension of the GAIW intrusion is reduced by up to 100 km and the monthly mean volume transport is decreased by 20% on average. Two actors that possibly contribute to the hindrance effects of tides in summer are (i) the tidal residual currents that propagate in a direction opposite to the pathway of the GAIW intrusion currents and (ii) the enhanced vertical mixing at the pycnocline and near the benthic topography of the BAM strait, which triggers more instabilities along the pathway of the intrusion.

KEYWORDS

tides, water exchange, mixing, the Red Sea, hindrance, the Gulf of Aden

1 Introduction

Tides play an important role in modulating the ocean circulation and water transformations, especially in the coastal oceans and gulfs, through tide-induced residual currents and tidal mixing processes (Aquad and Miller, 2008; Wang et al., 2017; Suanda et al., 2018). Using a high-resolution numerical model, Aquad and Miller (2008) showed that tides stir the water column in the coastal ocean of the Alaska Gulf,

thereby generating a horizontal density gradient. This gradient generates a geostrophic current that flows against the mean general circulation. Similarly, using numerical simulations, Callendar et al. (2011) reported that mesoscale dipoles are formed from coalescing tidal eddies when the tidal flow passes Cape St. James on the southern tip of Haida Gwaii, off the northern Pacific coast of Canada, providing a consistent source of coastal water to the interior of the subpolar gyre. Suanda et al. (2018) examined the effects of tides on the three-dimensional (3D) coastal dispersion processes in the Central Californian continental shelf during upwelling *via* a realistic, high-resolution simulation. They demonstrated that tides increase the horizontal and vertical dispersions by a factor of 2–3, suggesting the importance of including tides in the simulations of coastal passive tracer dispersion. Kida and Wijffels (2012) explored the impact of tidal mixing on the summertime sea surface temperature (SST) in the Western Indonesian Seas based on high-resolution numerical simulations. They reported that tidal mixing lowers the SST during summer through increased mixing with the upper thermocline water, which is then transported to the surface *via* the coastal upwelling process. Luneva et al. (2015) studied the effects of tides on the water mass mixing and sea ice in the Arctic Ocean. They conducted numerical simulations with and without tides and found that tides induced approximately 15% reduction in the volume of sea ice during the last decade. Moreover, they found that tidal interactions caused the redistribution of salinity through three processes: strong shear stresses in the interior waters, thicker subsurface ice–ocean and boundary layers, and an intensification of the quasisteady vertical motions of isopycnals. Wang et al., 2016; Wang et al., 2017 used an ocean model to investigate the impact of tidal mixing on water mass transformation and circulation in the South China Sea. They suggested that tidal mixing in the deep South China Sea is an important factor in strengthening the horizontal density gradient, which intensifies the basin-scale cyclonic circulation, causes vigorous overturning, and generates subbasin-scale eddies in the abyssal South China Sea.

The Red Sea is a semienclosed marginal sea. Its southern end is connected with the open ocean through the narrow Bab-al-Mandeb (BAM) strait. The sea has a relatively independent circulation system (Yao et al., 2014a; Yao et al., 2014b), making it an ideal basin for investigating the influence of tides on the basin's general circulations. The Red Sea spans an area of approximately 20° in latitude (from 10°N to 30°N) and approximately 10° in longitude (from 32°E to 42°E), which enables the development of a complete and composite circulation system of different scales, including the Gulf of Aden Intermediate Water (GAIW) intrusion (Sofianos and Johns, 2002), the deep water formation event in the north (Yao and Hoteit, 2018), a strong mesoscale eddy activity (Zhan et al., 2014; Zhan et al., 2018; Zhan et al., 2020), and small-scale internal solitary waves (ISWs) in the southern Red

Sea (Guo et al., 2016; Guo et al., 2021). The relatively small size of the Red Sea basin enables the implementation of a high-resolution numerical model capable of resolving small-scale processes such as baroclinic tides (Guo et al., 2018). The southern Red Sea is one of the energetic regions, and it is reported to be a hot spot of ISWs based on satellite images (Da Silva et al., 2012); the ISWs are possibly generated by a nonlinear steepening resulting from a large displacement of baroclinic tides (Guo et al., 2016). Using a nonhydrostatic, high-resolution simulation, Guo et al. (2018) showed that large-amplitude barotropic tides, which carry a large amount of energy, originating from the Gulf of Aden enter the Red Sea through the BAM strait and generate large baroclinic tides after interacting with the benthic topography. Observations at the Hanish Sill indicates the oscillations caused by these internal tides are up to 80 meters Morozov (2018). These baroclinic tides do not propagate far from their sources; instead, they dissipate quickly after their generation, resulting in considerable turbulence and mixing processes within the BAM (Guo et al., 2018), and form a location with the highest intensity in terms of baroclinic tidal energy. The associated tide-induced residual currents and mixing processes are expected to affect the exchange processes within the strait, and more generally, the entire Red Sea circulation.

The water exchange flows between the Red Sea and the Gulf of Aden are shown schematically in Figure 1B (adopted from Siddall et al. (2002)) and in the vertical profiles of temperature and salinity in Figure S1 (Supplementary Figure). In winter, a typical two-layer exchange structure with a fresh inflow from the Gulf of Aden overlying an outflow from the Red Sea is established. In summer, as the surface winds in the south Red Sea reverse from southeasterly to northwesterly Yao et al. (2014b), the circulation pattern is reversed and a three-layer structure is established following the upwelling process in the Gulf of Aden, with a surface outflow from the Red Sea overlying the subsurface intrusion of the GAIW and a much weaker deep outflow. Using long-term observations and numerical simulations of the strait, Sofianos and Johns, 2002; Sofianos and Johns, 2007; Yao et al., 2014a; Yao et al., 2014b and Xie et al. (2019) demonstrated the robustness of this seasonal overturning pattern. The GAIW intrusion in summer is an important feature of the Red Sea's general circulation. Because of its occurrence at the entrance of the strait, variations in GAIW may have important effects on the entire Red Sea circulation system (Yao et al., 2014a; Yao et al., 2014b). Further, GAIW transports nutrients to this oligotrophic basin (Raitsos et al., 2013; Raitsos et al., 2015), sustaining summer chlorophyll blooms along its southern coast (Dreano et al., 2016).

In this study, we examined the impact of tides on the water exchange at the BAM strait using the 3D nonhydrostatic MIT general circulation model (MITgcm) simulations with and without tidal forcing. Accounting for tides, the simulation suggests an improved reproduction of the GAIW intrusion

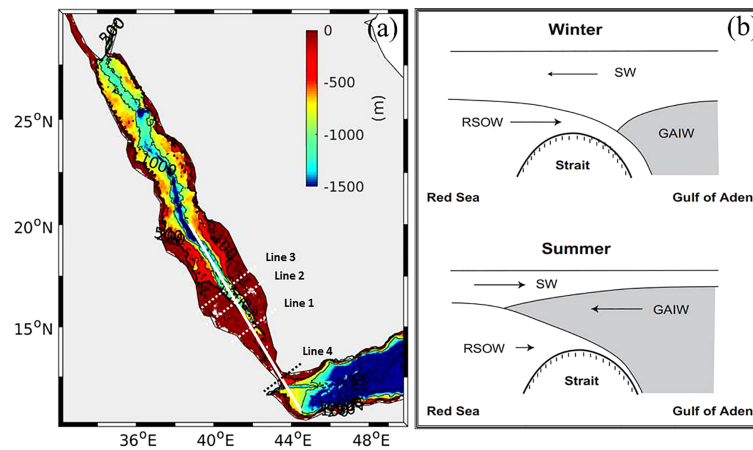


FIGURE 1

(A) Bathymetry of the Red Sea. The white line indicates the along-axis transect of the summer intrusion of GAIW and dashed lines represent the cross-sections; (B) the schematic figure of the stratification structure at the BAM strait in Winter (upper panel) and Summer (lower panel). Panel (B) is adopted from Siddall et al. (2002).

compared with the observations; the volume transport of GAIW through the BAM strait decreased by approximately 20% on average, revealing the hindrance effect of tides. In winter, the influence of tides on the water exchange is insignificant. Herein, we show that the hindrance effect in summer is due to the tidal residual currents that flow in a direction opposite to the intrusion pathway in the southern Red Sea and due to the enhanced tidal mixing at the BAM strait. The remainder of this paper is organized as follows. The model configuration is described in Section 2, and the validation of the model simulations through comparisons with available observations is presented in Section 3. The main results of tidal impact on the water exchanges, focusing on the GAIW intrusion, in particular, are described in Section 4. The mechanisms behind the tidal hindrance effects are analyzed and discussed in Section 5. A summary of the main findings is provided in Sections 6.

2 Model configuration

Numerical simulations of the Red Sea general circulation were conducted using the MITgcm. This model has been successfully used to describe the basin overturning circulation (Yao et al., 2014a; Yao et al., 2014b), seasonal variability (Zhan et al., 2014), and kinetic energy budget (Zhan et al., 2016) of mesoscale eddies and to develop ensemble data assimilation capabilities (Toye et al., 2017; Toye et al., 2018; Sanikommu et al., 2020). The MITgcm was further implemented with tidal forcing to describe the characteristics of baroclinic tides in the Red Sea (Guo et al., 2018), revealing four main energetic regions of baroclinic tides.

The model's domain includes all of the Red Sea basin, the Gulf of Suez, the Gulf of Aqaba, and most of the Gulf of Aden,

where an open boundary is configured at 50°E (Figure 1A). The bottom topography is derived from the General Bathymetric Chart of the Oceans (GEBCO) digital atlas, with 30-arc-second intervals. Some adjustments were applied to the bathymetry near the BAM strait in shallow areas (water depths: 100–138 m) of the Hanish Sill region, according to Sea Chart No. 3661 (3rd edition, printed in May 2003). Coastline features were improved on the basis of the Global Self-consistent, Hierarchical, High-resolution Geography Database. The model was configured with a horizontal resolution of 0.01° (~ 1km), and it had 50 vertical layers with a minimum thickness of 4 m near the surface and a maximum thickness of 300 m near the bottom of the seafloor. A nonslip condition was imposed at the bottom boundary with a spatially constant, quadratic drag coefficient C_d of 0.002. Atmospheric forcings were extracted from the European Reanalysis-Interim (ERA-Interim) of the European Centre for Medium-range Weather Forecasts (ECMWF) (Dee et al., 2011) available at a 0.75° spatial and six-hourly temporal resolutions. The lateral daily boundary conditions of horizontal velocity, temperature, and salinity were extracted from the monthly 1/3° German contribution of the project Estimating the Circulation and Climate of the Ocean Version 2 (GECCO2) ocean global reanalysis (Köhl, 2015).

There are two standard approaches to account for tides or tidal effects. The first is to add tide-induced diffusivity, representing tide-induced mixing, through conversion of baroclinic tides energy dissipation rates (Wang et al., 2016; Wang et al., 2017). The other is to directly force the model with barotropic tides at the open boundaries; tidal mixing is estimated using a certain parameterization scheme (Auaud and Miller, 2008; Suanda et al., 2018). The two approaches have their own merits and shortcomings. The first approach provides

relatively accurate tidal mixing estimate but does not account for time variations nor direct tidal residual currents. The second one accounts for time variations and the tidal residual currents but the parameterization scheme does not fully resolve the tidal mixing process (Suanda et al., 2018). We adopted the second approach in this study to resolve the important seasonal stratification variations at the BAM strait. The tidal forcing was implemented by importing barotropic currents from the eastern open boundary (set at 50°E) in the Gulf of Aden. The amplitudes and phases of the tidal currents were extracted from the inverse barotropic tidal model TPXO 7.2 Indian Ocean (Egbert and Erofeeva, 2002), available at a horizontal resolution of 1/16°. Eight major tidal components of semidiurnal and diurnal frequencies (M2, S2, N2, K2, K1, O1, P1, and Q1, ordered according to their amplitudes in the Red Sea) were included. To account for the 18.6-year astronomical tide-generating potential cycle, a nodal correction (Pawlowicz et al., 2002) was applied to the derivations of the amplitudes and phases of the barotropic currents, which are essential for obtaining accurate barotropic tidal simulations. The nonlocal K-profile parameterization scheme (Large et al., 1994) was adopted to resolve the small-scale processes and vertical mixing. A detailed validation of barotropic tides against observations is presented in Guo et al. (2018).

The analysis of the impacts of tidal forcing on the water exchanges at the BAM strait was based on the simulations results

of two model runs with and without tidal forcing. Both simulations started from December 1994, with initial conditions from an existing long-term 1 km Red Sea model simulation (Krokos et al., 2021). The run without tides was integrated for three years until December 1997. In comparison, the run with tides was integrated until the end of May 1996, after which the tides were removed and the simulation resumed until December 1997. A comparison of the water exchanges from the two runs between June 1996 and December 1997 suggest that the tidal induced large scale circulation adjustments become not significant after about 3-4 months, as seen Figure S2 (Supplementary Figure).

3 Comparisons with observations

The model outputs were first evaluated against the available *in situ* observations to validate the simulations results. Observations from a one-year time series temperature and salinity profiles were collected at the Hanish Sill in the BAM strait from June 1995 to November 1996 (Murray and Johns, 1997; Sofianos et al., 2002). The data were filtered using a 20-day low-pass filter, as shown in Figure 2A1. The corresponding model outputs are plotted in Figure 2A2 for the run without tides and in Figure 2A3 for the run with tides. Both runs thoroughly reproduced the intrusion process of GAIW near the Hanish Sill. In the simulation, GAIW intrusion started from

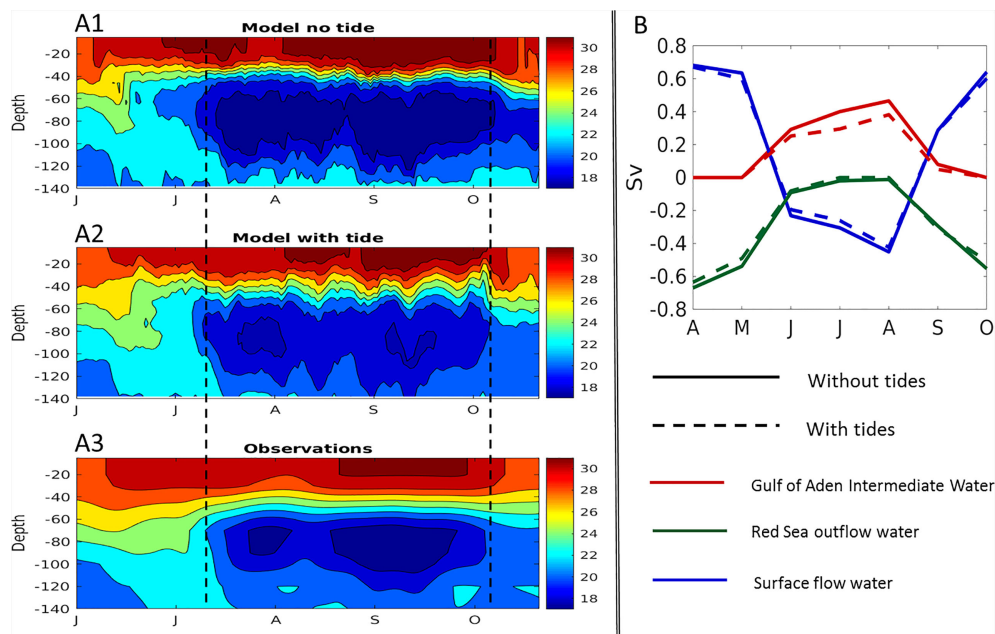


FIGURE 2

A comparison of model results and observations. Panels (A1), (A2), and (A3) represent the Hovmöller diagrams of the temperature field from the model run without tides, the model run with tides and the observations, respectively. The data in (A3) is run through a low-pass filter with a 20-day frequency. Panel (B) plots the monthly mean layer transport volumes at the BAM strait from the model outputs.

the beginning of July of 1995 in the run with tides and slightly earlier in the run without tides (Figure 2A2); it ceased in the middle of October in the run with tides, and it ceased slightly earlier in the run without tides. The other noticeable feature in the observations is that the coldest water masses (below 18°C) show two intrusion periods, with a shorter duration around the end of July and a longer duration from the middle of August to the end of September. Both runs did not adequately reproduce this intermittent intrusion process, which might not be well described by the atmospheric forcing of the

ECMWF. The run without tides showed the continuous presence of the coldest water masses, whereas the run with tides did not show the second period. The run without tides seemed to overestimate the intrusion of GAIW at Hanish Sill; the run with tides reproduced this process better, although it slightly underestimated the observations. The difference in winter exchange between the two runs is insignificant; both the runs reproduce the two-layer exchange flow and show a reasonable agreement with the observations.

A quantitative estimate of the volume transport of the water mass exchange at the different layers was reported by Sofianos and Johns (2002) based on direct observations from Murray and Johns (1997). This estimate revealed that the GAIW intrusion lasts for four months (June–September), with an average of

0.22Sv entering the Red Sea basin. The same volume transport estimated from the monthly mean model outputs is plotted in Figure 2B. The solid curves indicate the results of the run without tides, and the dashed curves indicate those of the run with tides. The two runs exhibit small differences in the transport volumes of the Red Sea surface flow and the Red Sea overflow and a relatively larger mismatch in the transport volume of GAIW. The average transport volume of GAIW in the run without tides is 0.30Sv while that in the run with tides is 0.24Sv, suggesting a closer agreement with the observations for the run with tides. A detailed analysis of the volume transport is shown in Section 4.4.

4 Tidal influence on the intrusion of GAIW

The tidal influence on the water exchanges in the BAM strait was examined by comparing the differences between the runs with and without tides. In winter, the differences in water exchanges between the runs were insignificant. However, there was a large difference between the runs in the reproduction of the GAIW intrusion in summer. Possible reasons and mechanisms for this are discussed in Section 5. In this section, we focus on the effects of tides on the GAIW intrusion and compare the results obtained in the two runs in terms of the along-axis extensions of the GAIW, horizontal extension of GAIW at the mid-layer depth, cross-axis transect profiles, and volume transports based on tracer-tracking experiments.

4.1 Along-axis extension

Figure 3 shows a comparison of the along-axis extension of the summer intrusion of GAIW between the two runs. The location of the transect profile is indicated by the solid white line in Figure 1A. The contours indicate the monthly mean potential temperature fields obtained from the simulations results. The dark blue color represents the water mass of GAIW, which is defined in this study as the water with a potential temperature of less than 20°C (indicated by the white dashed curves). In April and May, the GAIW mainly remains in the Gulf of Aden; in June, it gradually accumulates and starts to penetrate through the strait. In July, August, and September, GAIW intrusion occurs and the stratification within the BAM strait exhibits a three-layer structure: colder and fresher GAIW intrusion in the middle and the warmer outflow Red Sea water at the surface and bottom of the water column. In October and November, GAIW retreats to the Gulf of Aden and the stratification within the strait transforms back to the two-layer structure: the surface water outflows to the Gulf of Aden and deep water inflows to the Red Sea. Both runs reproduce the Red Sea–Gulf of Aden water exchange processes but exhibit pronounced differences in the along-axis extension of the GAIW. In the run without tides, the intrusion reaches up to 17.8°N, as indicated by the monthly mean potential temperature field for October. In the run with tides, the along-axis extension of the intrusion only reaches the end of the strait, i.e., to approximately 17.0°N (Figure 3, Oct), suggesting a clear hindrance effect of the tides on the intrusion of GAIW.

4.2 Horizontal extension at the mid-layer depth

The horizontal view of the extension of the GAIW is shown in Figure 4. The top panels show the monthly mean temperature field at a depth of 63 m in August, and the bottom panels show the same information for September. Both runs reproduce the general picture of the intrusion process thoroughly, showing the GAIW entering the Red Sea and then propagating northward, with a slight inclination toward the eastern side of the axial trough of the Red Sea basin. However, there are clear differences between the two runs. In August, the GAIW reaches close to 16.5°N in the run without tides, whereas it only approaches near 16.0°N in the run with tides. In September, the GAIW reaches beyond 17.0°N in both the runs, but the water masses exhibit colder temperatures in the run without tides. A horizontal view of the intrusion shows a wider horizontal coverage in the run without tides. Another noticeable feature is that the boundaries between the water masses of GAIW and Red Sea water are less pronounced in the run with tides; in Figure 4, this phenomenon is indicated by the blurry boundaries between the blue and red

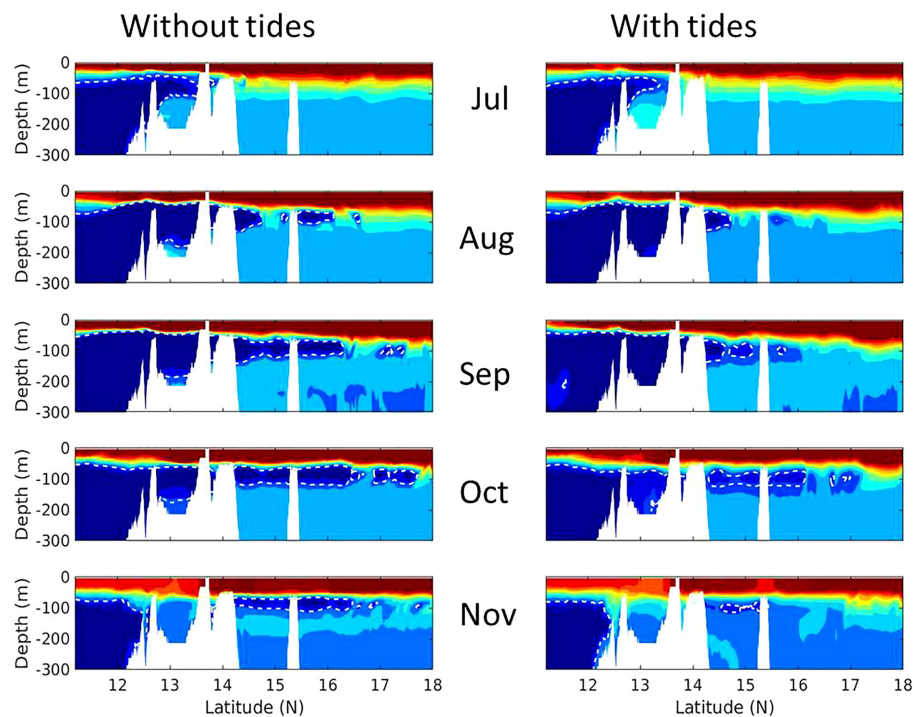


FIGURE 3

The comparisons of the along-axis extension of the summer intrusion of GAIW between the runs without tides (left panels) and with tides (right panels). The time variation of the monthly-mean potential temperature is shown from July (top) to November (bottom). The white dashed curves show the isotherms of 20°C as an indication of GAIW.

zones or areas in the right-hand side panels, suggesting that more intense mixing may be occurring near the fronts of intruded flow in the run with tides.

4.3 Cross-axis transects profiles

Considering the differences in the along-axis extension of the summer intrusion of GAIW between the two runs, we further analyzed the potential temperature fields of the cross-axis transects profiles. Sofianos and Johns (2007) and Yao et al., 2014b; Yao et al., 2014a reported that the intrusion flows slightly to the east when it extends northward. This 3D feature can be observed in the monthly mean potential temperature fields of the cross-axis transects shown in Figure 5. The transects are indicated by white dashed lines in Figure 1A for September.

Along transect Line 1, with the middle point at approximately 13.87°N, the intrusion of GAIW is obvious in both the runs. The pattern and the three-layered structure within the transects are similar; however, the intermediate water is 1 to 2 degree colder in the run without tides than the run with tides, suggesting that more water intrusion occurs in the run without tides. Along transect Line 2, with the middle point at approximately 15.48°N, a clear three-layer stratification is seen

in the run without tides. By contrast, only a tilted isotherm is observed in the run with tides, indicating that the intrusion ends with the two-layered structure near the transect. Along transect Line 3, with the middle point at approximately 16.28°N, the intrusion still can be observed as a weak three-layered structure within the central area of the transect in the run without tides; this structure is not reproduced in the run with tides.

4.4 Volume transport

For a quantitative assessment of the impact of the tides, the volume transport of the intruded GAIW was estimated following the method of Xie et al. (2019), on the basis of the monthly mean velocity and potential temperature along the transects of the cross-line, indicated by the black dashed line in Figure 1A. The GAIW is defined as the water mass with a potential temperature of less than 20°C and is indicated by dark blue color in Figure 2. The results suggest that in the run with tides, the monthly mean transport volumes of GAIW are 25.23, 29.53, 38.02, and 5 (10–2Sv) in June, July, August, and September, and in the run without tides, the transport volumes are 29.28, 40.07, 46.58, and 8 (10–2Sv), respectively. Thus, by including tides in the simulation, the volumes are reduced by 0.04, 0.11, 0.08, and 0.03 (10–2Sv) in

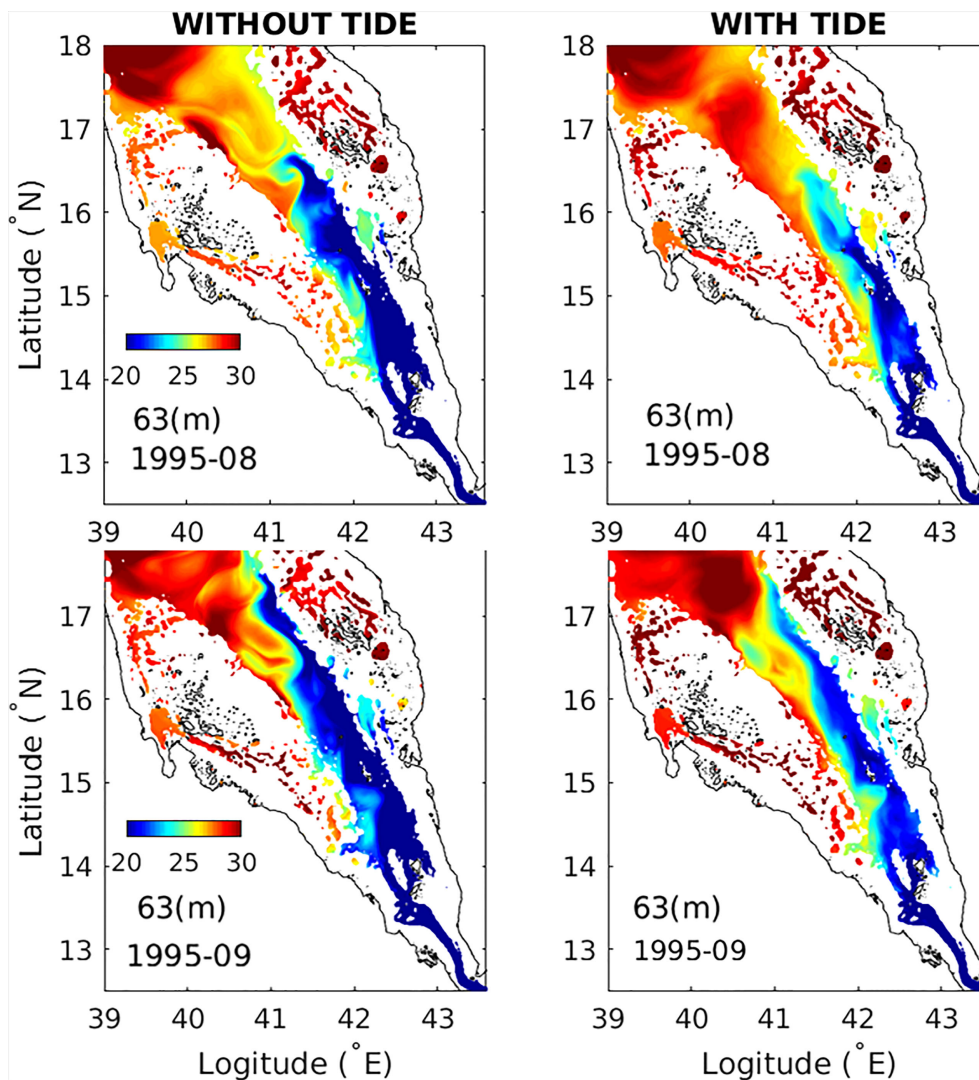


FIGURE 4
 A comparison of the horizontal extension of the summer intrusion of GAIW at mid-depth (63 m) between the runs without tides (left panels) and with tides (right panels). The time variations of the monthly-mean potential temperature are shown for August and September in the upper panels and lower panels, respectively.

June, July, August, and September, respectively. On average, the transport volume decreased by around 20%, with the average transport volumes of 0.3098 Sv and 0.2449 Sv in the runs without and with tides, respectively.

4.5 Tracer experiments

We conducted passive tracer-tracking experiments to quantitatively investigate the impact of tides on the intrusion of GAIW. In the runs with and without tides, passive tracers were continuously released from the Gulf of Aden by relaxing and normalized to a fixed value of 100. The tracers were tracked after

the GAIW intrusion began. To explain the intrusion process, Figure 6 shows five snapshots of the horizontal view of tracers in the southern Red Sea at 100-m depth. Similar to the differences between the two runs as revealed from the results of the potential temperature field, there is a clear reduction in the number of tracers observed in the run with tides and the maximum northward extension of the intrusion shows a difference of approximately 100 km between the two runs in the last snapshot of September. In the run without tides, the tracers reach approximately 17.3°N because of the northward-propagating current and the mesoscale eddies, whereas in the run with tides, it remains near 16°N. The bottom panel of Figure 6 shows the time series of the accumulated spatial mean tracer numbers; this panel shows that the difference

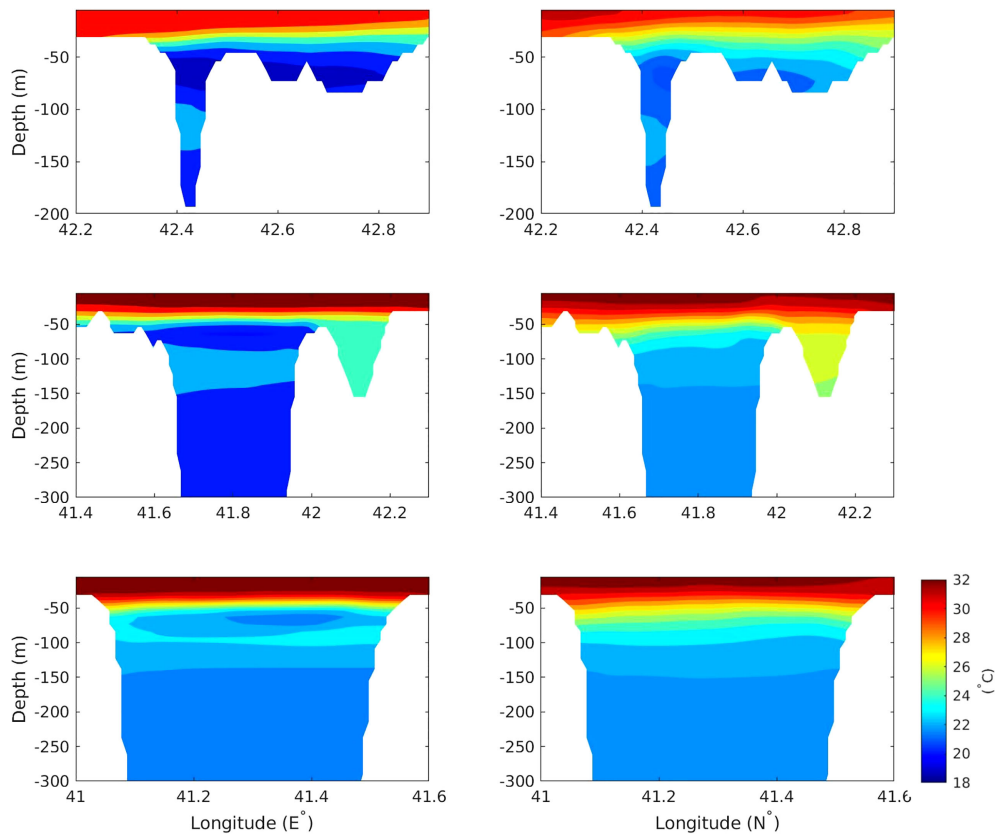


FIGURE 5

The comparisons of the cross-section extension of the summer intrusion of GAIW between the runs without tides (left panels) and with tides (right panels). The three panels from top to bottom represents the potential temperature fields of three cross-sections indicated by white dash-lines (Lines 1, 2 and 3) in Figure 1A.

between the two runs appears at the beginning of May and develops slowly through June, July, and August, before reaching the maximum of approximately 3×10^{-11} mol/m³ in mid-September. The difference remains relatively constant at this maximum value after October.

5 Discussion

Previous studies indicated that tides affect the general circulations mainly through the tidal residual currents and tidal mixing process (Aquad and Miller, 2008; Xuan et al., 2016; Suanda et al., 2018). The tidal residual currents can directly influence and modulate the background general circulation currents or mesoscale eddies, while tidal mixing can affect the water mass transformation through modulation of the diffusivity and viscosity (Wang et al., 2016; Wang et al., 2017). To investigate the potential mechanism behind the tidal hindrance effects on GAIW intrusion in the BAM strait, we examined the tidal residual currents and tidal mixing.

5.1 Tidal residual currents

We first examined the Eulerian residual currents because the Stokes drift currents are more closely related to material transport (Xuan et al., 2016). The residual currents were calculated on the basis of one-year continuous model outputs by averaging the current time series. The spatial distribution of the vertically averaged tidal residual currents in the southern Red Sea is shown in Figure 7. A strong southeastward-propagating current along the east of the trough and an opposite current along the west of the trough are noticeable in the southern Red Sea near 16°N. The maximum tidal residual current velocity can reach up to approximately 0.1 m/s. A comparison of Figure 7 with Figure 4 reveals that the location of the southeastward current is opposite to the northwest intrusion of GAIW in August and September. This may potentially weaken the intrusion current speed and hinder the intrusion process; this finding is consistent with the difference revealed in the simulation results. In the wintertime, the tidal residual currents do not have a large impact on the water exchange in

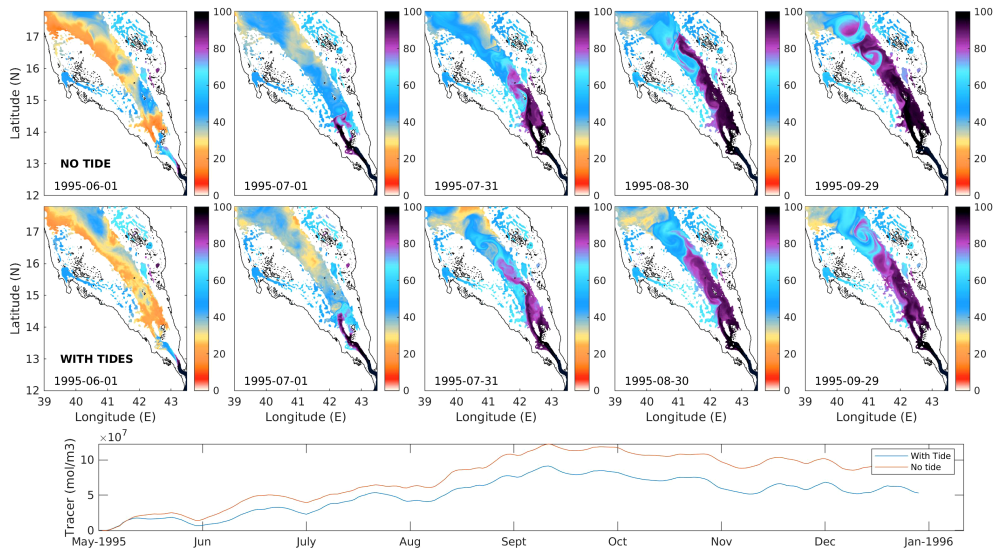


FIGURE 6
 Five snapshots of the horizontal view of tracers in the southern Red Sea at the depth of 100 m in run without tides (top panels) and with tides (mid panels). Bottom panel shows the time series of the accumulated spatial mean of tracer numbers in the southern Red Sea, with red curve indicating run without tides and blue for run with tides.

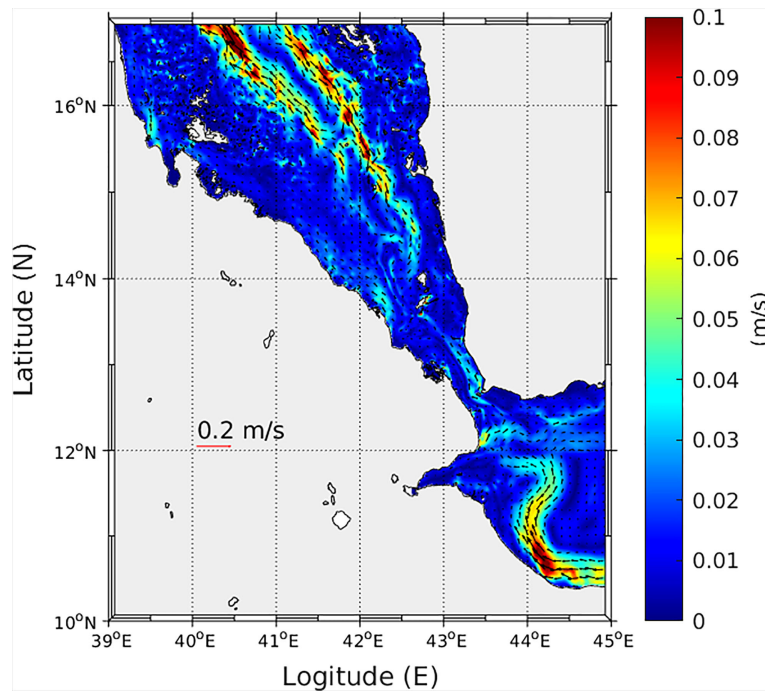


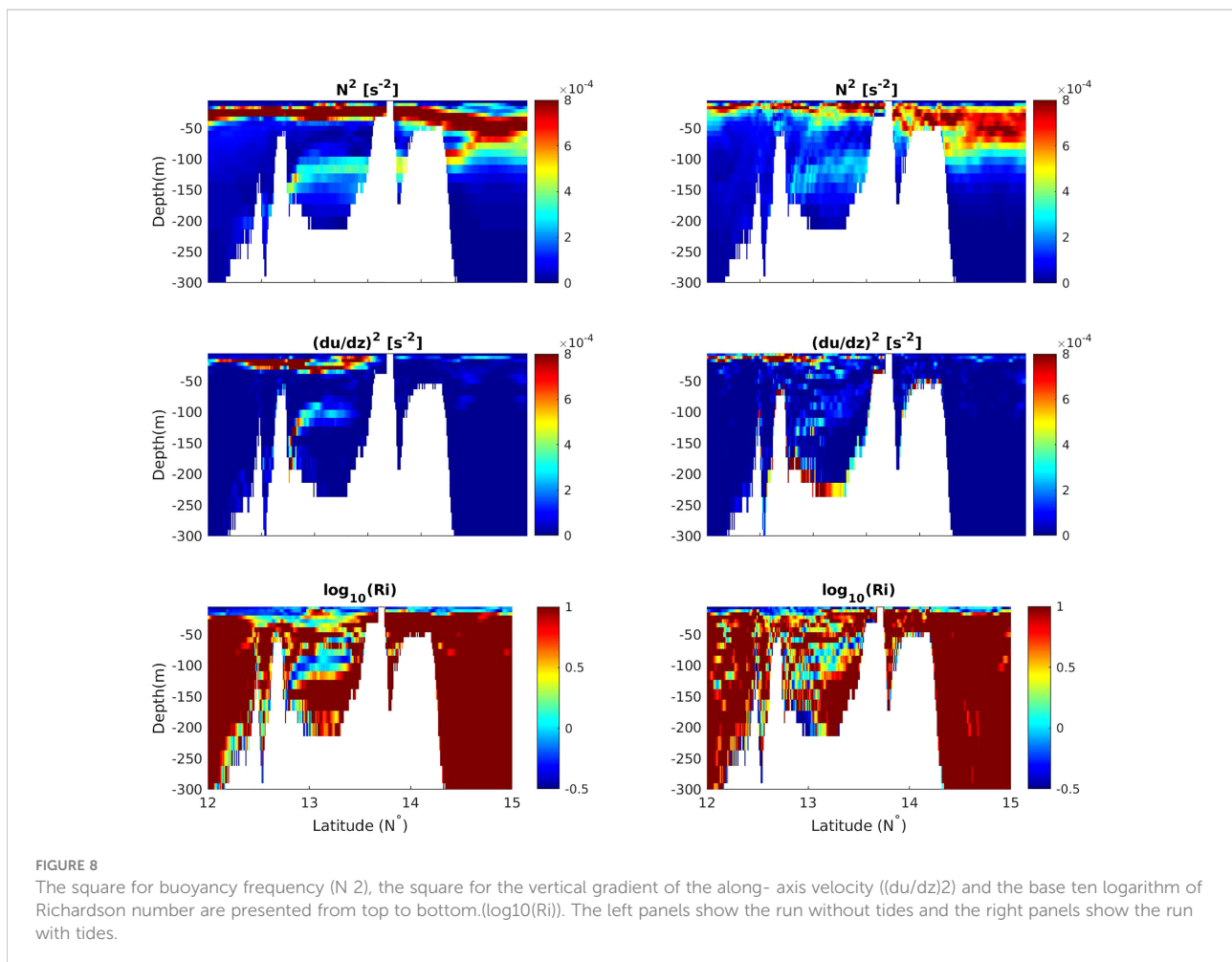
FIGURE 7
 Tidal residual currents at the BAM strait and the southern Red Sea.

the BAM strait because the residual current in the opposite direction, along the west of the trough, may cancel the effect of the northward-propagating residual current. The tidal residual currents not only influence the water exchanges in the strait but also can directly alter the local current structure. The twin tidal residual currents in the southern Red Sea and the strong current along the west coast of the Gulf of Aden enhance the local clockwise current and can generate submesoscale eddies or gyres.

5.2 Tidal mixing

Tidal mixing can induce more vertical instabilities in the water column, which can modulate the water mass transformation and influence the large-scale circulation. We can examine the submesoscale tidal mixing based on Figure 8, which compares the square of buoyancy frequency (N^2), the square of the vertical gradient of the along-axis velocity ($(du/dz)^2$), and the base-10 logarithm of the Richardson number ($\log_{10}(Ri)$) between the runs with (left panels) and without tides (right

panels). A considerable difference can be observed in the buoyancy frequency fields. In the run without tides, the interfaces between the layers are thin and the buoyancy frequency is relatively high. In the run with tides, the interfaces are thick but scattered with lower buoyancy frequency. These scattering effects may be related to the baroclinic tides, which interfere with the thermocline and generate smaller disturbances. These disturbances likely increase the friction between the interfaces and prevent the GAIW intrusion from extending northward. The vertical gradient of the along-axis velocity shows larger values near the interfaces in the run without tides. At the interfaces, the directions of the currents are reversed: the surface and bottom water propagate southward, whereas the intermediate water propagates northward. However, these reversed currents are not likely to generate small-scale vertical mixing because they remain dynamically balanced. In the run with tides, larger values occur near the bottom, indicating that baroclinic tides are generated during the interactions between the barotropic tides and benthic topography. These baroclinic tides dissipate more energy from the intruded flow. Similar features are observed in



the comparison of the $\log_{10}(Ri)$. A more complex structure and smaller values of $\log_{10}(Ri)$ occur in the run with tides near the mid-depth and near the bottom, indicating that more instability is triggered in the water column when tides are included. In the run without tides, the intrusion shows a clearer three-layered structure, with small Ri values near the interfaces of the water masses. These small Ri values are not likely to generate unstable overturning or mixing processes; conversely, the more scattered small Ri values in the run with tides indicate the intensified mixing processes along the interfaces. Although tidal mixing also influences the interface of the two-layered stratification in wintertime, the intensity of the influence is considerably less than that in summertime; further, the water exchanges are not significantly affected in the wintertime.

6 Summary

There is a growing interest in exploring whether and how small-scale processes such as mixing and turbulence affect large-scale processes and general circulations. Herein, we presented a case study of the influence of tides on the water exchange between the Red Sea and the Gulf of Aden through the BAM strait based on numerical simulations. These simulations were validated using available observations. The analysis of the simulation outputs revealed the hindrance effect of tides on the summer intrusion of the GAIW into the Red Sea.

The Red Sea simulations were conducted using a 1-km nonhydrostatic MITgcm. By configuring the model with and without a tidal forcing mechanism, we observed that the GAIW intrusion during summertime is strongly affected by tides. When the tides are included in the simulation, the along-axis northward extension of the intrusion reduces by approximately one degree and the transported volumes of GAIW decrease by 20% on average. Analyses of the tidal residual currents and the stability of the water column and vertical mixing indicate that the most likely causes of the hindrance effects of the tides are the southward-propagating residual currents in the southern Red Sea and the enhancement of the vertical movements along the thermocline and near the benthic topography. Tidal mixing increases the roughness of the interfaces between the layers, thereby enhancing the friction and hindering the intrusion.

This study showcases that small-scale, high-frequency physical processes can influence the large-scale processes in the Red Sea. Because of the limitation of computation resources, we performed only a one-year simulation run. More evidence and important influences of tides on the general circulations, such as the properties of eddy activities and deep-sea water mass transformations in the Red Sea can be revealed by longer simulations that will be conducted in the future. The substantial tidal impact on the general circulation of the Red Sea reported herein can contribute toward the improvement of

mixing parameterizations for regional and global climate model simulations.

Data availability statement

The original contributions presented in the study are included in the article/[Supplementary Material](#). Further inquiries can be directed to the corresponding author.

Author contributions

The authors confirm contribution to the paper as follows: study conception and design: DG, FY, PZ, and IH. Data collection: DG and GK; analysis and interpretation of results: DG, GK, PZ, and IH. All authors contributed to the article and approved the submitted version.

Acknowledgments

The reported research was supported by the Office of Sponsored Research (OSR) at King Abdullah University of Science and Technology (KAUST) under the Competitive Research Grants (CRG) program (Grants # FCC/1/1973-01-01). This research made use of the computational resources of the KAUST Supercomputing Laboratory (SHAHEEN).

Conflict of interest

The authors declare that the research was conducted in the absence of any commercial or financial relationships that could be construed as a potential conflict of interest.

Publisher's note

All claims expressed in this article are solely those of the authors and do not necessarily represent those of their affiliated organizations, or those of the publisher, the editors and the reviewers. Any product that may be evaluated in this article, or claim that may be made by its manufacturer, is not guaranteed or endorsed by the publisher.

Supplementary material

The Supplementary Material for this article can be found online at: <https://www.frontiersin.org/articles/10.3389/fmars.2022.964097/full#supplementary-material>

References

- Auad, G., and Miller, A. J. (2008). The role of tidal forcing in the gulf of alaska's circulation. *Geophysic Res. Lett.* 35, L04603. doi: 10.1029/2007GL032727
- Callendar, W., Klymak, J., and Foreman, M. (2011). Tidal generation of large sub-mesoscale eddy dipoles. *Ocean Sci.* 7, 487–502. doi: 10.5194/os-7-487-2011
- Da Silva, J. C., Magalhaes, J. M., Gerkema, T., and Maas, L. R. (2012). Internal solitary waves in the red sea: an unfolding mystery. *Oceanography* 25, 96–107. doi: 10.5670/oceanog.2012.45
- Dee, D., Uppala, S., Simmons, A., Berrisford, P., Poli, P., Kobayashi, S., et al. (2011). The era-interim reanalysis: Configuration and performance of the data assimilation system. *Q. J. R. Meteorol. Soc.* 137, 553–597. doi: 10.1002/qj.828
- Dreano, D., Raitsos, D. E., Gittings, J., Krokos, G., and Hoteit, I. (2016). The gulf of aden intermediate water intrusion regulates the southern red sea summer phytoplankton blooms. *PLoS One* 11, e0168440. doi: 10.1371/journal.pone.0168440
- Egbert, G. D., and Erofeeva, S. Y. (2002). Efficient inverse modeling of barotropic ocean tides. *J. Atmospheric Oceanic Technol.* 19, 183–204. doi: 10.1175/1520-0426(2002)019<0183:EIMOBO>2.0.CO;2
- Guo, D., Akylas, T. R., Zhan, P., Kartadikaria, A., and Hoteit, I. (2016). On the generation and evolution of internal solitary waves in the southern red sea. *J. Geophysic Research: Oceans* 121, 8566–8584. doi: 10.1002/2016JC012221
- Guo, D., Kartadikaria, A., Zhan, P., Xie, J., Li, M., and Hoteit, I. (2018). Baroclinic tides simulation in the red sea: Comparison to observations and basic characteristics. *J. Geophysic Research: Oceans* 123, 9389–9404. doi: 10.1029/2018JC013970
- Guo, D., Zhan, P., and Hoteit, I. (2021). Three-dimensional simulation of shoaling internal solitary waves and their influence on particle transport in the southern red sea. *J. Geophysic Research: Oceans* 126, e2020JC016335. doi: 10.1029/2020JC016335
- Kida, S., and Wijffels, S. (2012). The impact of the indonesian throughflow and tidal mixing on the summertime sea surface temperature in the western indonesian seas. *J. Geophysic Research: Oceans* 117, C09007. doi: 10.1029/2012JC008162
- Köhl, A. (2015). Evaluation of the gecco2 ocean synthesis: transports of volume, heat and freshwater in the atlantic. *Q. J. R. Meteorol. Soc.* 141, 166–181. doi: 10.1002/qj.2347
- Krokos, G., Cerovec'ki, I., Zhan, P., Hendershott, M., and Hoteit, I. (2021). Seasonal evolution of mixed layers in the red sea and the relative contribution of atmospheric buoyancy and momentum forcing. (Vol. 1–44). Retrieved from <http://arxiv.org/abs/2112.08762>.
- Large, W. G., McWilliams, J. C., and Doney, S. C. (1994). Oceanic vertical mixing: a review and a model with a nonlocal boundary layer parameterization. *Rev. geophysics* 32, 363–403. doi: 10.1029/94RG01872
- Luneva, M. V., Aksenov, Y., Harle, J. D., and Holt, J. T. (2015). The effects of tides on the water mass mixing and sea ice in the arctic ocean. *J. Geophysic Research: Oceans* 120, 6669–6699. doi: 10.1002/2014JC010310
- Morozov, E. G. (2018). *Oceanic internal tides: Observations, analysis and modeling* (Cham: Springer International Publishing).
- Murray, S. P., and Johns, W. (1997). Direct observations of seasonal exchange through the bab el mandab strait. *Geophysic Res. Lett.* 24, 2557–2560. doi: 10.1029/97GL02741
- Pawlowicz, R., Beardsley, B., and Lentz, S. (2002). Classical tidal harmonic analysis including error estimates in matlab using t tide. *Comput. Geosci* 28, 929–937. doi: 10.1016/S0098-3004(02)00013-4
- Raitsos, D. E., Pradhan, Y., Brewin, R. J., Stenchikov, G., and Hoteit, I. (2013). Remote sensing the phytoplankton seasonal succession of the red sea. *PLoS One* 8, e64909. doi: 10.1371/journal.pone.0064909
- Raitsos, D. E., Yi, X., Platt, T., Racault, M.-F., Brewin, R. J., Pradhan, Y., et al. (2015). Monsoon oscillations regulate fertility of the red sea. *Geophysic Res. Lett.* 42, 855–862. doi: 10.1002/2014GL062882
- Sanikomm, S., Toye, H., Zhan, P., Langodan, S., Krokos, G., Knio, O., et al. (2020). Impact of atmospheric and model physics perturbations on a high-resolution ensemble data assimilation system of the red sea. *J. Geophysic Research: Oceans* 125, e2019JC015611. doi: 10.1029/2019JC015611
- Siddall, M., Smeed, D., Mathiessen, S., and Rohling, E. (2002). "Exchange flow between the red sea and the gulf of aden," in *The 2nd meeting on the physical oceanography of Sea straits* (Villefranche (Citeseer)), 203–206.
- Sofianos, S. S., and Johns, W. E. (2002). An oceanic general circulation model (ogcm) investigation of the red sea circulation, 1. exchange between the red sea and the indian ocean. *J. Geophysic Research: Oceans* 107, 3066. doi: 10.1029/2001JC001185
- Sofianos, S. S., and Johns, W. E. (2007). Observations of the summer red sea circulation. *J. Geophysic Research: Oceans* 112, C06025. doi: 10.1029/2006JC003886
- Sofianos, S., Johns, W. E., and Murray, S. (2002). Heat and freshwater budgets in the red sea from direct observations at bab el mandeb. *Deep Sea Res. Part II: Topical Stud. Oceanog* 49, 1323–1340. doi: 10.1016/S0967-0645(01)00164-3
- Suanda, S. H., Feddersen, F., Spydell, M. S., and Kumar, N. (2018). The effect of barotropic and baroclinic tides on three-dimensional coastal dispersion. *Geophysic Res. Lett.* 45, 11–235. doi: 10.1029/2018GL079884
- Toye, H., Kortas, S., Zhan, P., and Hoteit, I. (2018). A fault-tolerant hpc scheduler extension for large and operational ensemble data assimilation: Application to the red sea. *J. Comput. Sci.* 27, 46–56. doi: 10.1016/j.jocs.2018.04.018
- Toye, H., Zhan, P., Gopalakrishnan, G., Kartadikaria, A. R., Huang, H., Knio, O., et al. (2017). Ensemble data assimilation in the red sea: sensitivity to ensemble selection and atmospheric forcing. *Ocean Dynamics* 67, 915–933. doi: 10.1007/s10236-017-1064-1
- Wang, X., Liu, Z., and Peng, S. (2017). Impact of tidal mixing on water mass transformation and circulation in the south china sea. *J. Phys. Oceanog* 47, 419–432. doi: 10.1175/JPO-D-16-0171.1
- Wang, X., Peng, S., Liu, Z., Huang, R. X., Qian, Y.-K., and Li, Y. (2016). Tidal mixing in the south china sea: An estimate based on the internal tide energetics. *J. Phys. Oceanog* 46, 107–124. doi: 10.1175/JPO-D-15-0082.1
- Xie, J., Krokos, G., Sofianos, S., and Hoteit, I. (2019). Interannual variability of the exchange flow through the strait of bab-al-mandeb. *J. Geophysic Research: Oceans*, 124, 1988–2009. doi: 10.1029/2018JC014478
- Xuan, J., Yang, Z., Huang, D., Wang, T., and Zhou, F. (2016). Tidal residual current and its role in the mean flow on the changjiang bank. *J. Mar. Syst.* 154, 66–81. doi: 10.1016/j.jmarsys.2015.04.005
- Yao, F., and Hoteit, I. (2018). Rapid red sea deep water renewals caused by volcanic eruptions and the north atlantic oscillation. *Sci. Adv.* 4, eaar5637. doi: 10.1126/sciadv.aar5637
- Yao, F., Hoteit, I., Pratt, L. J., Bower, A. S., Köhl, A., Gopalakrishnan, G., et al. (2014a). Seasonal overturning circulation in the red sea: part 2. winter circulation. *J. Geophysic Research: Oceans* 119, 2263–2289. doi: 10.1002/2013JC009004
- Yao, F., Hoteit, I., Pratt, L. J., Bower, A. S., Zhai, P., Köhl, A., et al. (2014b). Seasonal overturning circulation in the red sea: part 1. model validation and summer circulation. *J. Geophysic Research: Oceans* 119, 2238–2262. doi: 10.1002/2013JC009331
- Zhan, P., Gopalakrishnan, G., Subramanian, A. C., Guo, D., and Hoteit, I. (2018). Sensitivity studies of the red sea eddies using adjoint method. *J. Geophysic Research: Oceans* 123, 8329–8345. doi: 10.1029/2018JC014531
- Zhan, P., Guo, D., and Hoteit, I. (2020). Eddy-induced transport and kinetic energy budget in the arabian sea. *Geophysic Res. Lett.* 47, e2020GL090490. doi: 10.1029/2020GL090490
- Zhan, P., Subramanian, A. C., Yao, F., and Hoteit, I. (2014). Eddies in the red sea: A statistical and dynamical study. *J. Geophysic Research: Oceans* 119, 3909–3925. doi: 10.1029/2013JC018015
- Zhan, P., Subramanian, A. C., Yao, F., Kartadikaria, A. R., Guo, D., and Hoteit, I. (2016). The eddy kinetic energy budget in the red sea. *J. Geophysic Research: Oceans* 121, 4732–4747. doi: 10.1002/2015JC011589